CARBON 48 (2010) 1498–1507

available at www.sciencedirect.com

ScienceDirect

journal homepage: www.elsevier.com/locate/carbon

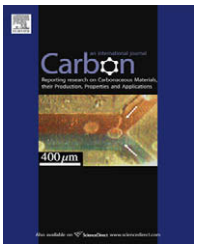

Structural and morphological control of aligned nitrogen-doped carbon nanotubes

Hao Liu [a], *Yong Zhang* [a], *Ruying Li* [a], *Xueliang Sun* [a,*], *Sylvain Désilets* [b], *Hakima Abou-Rachid* [b,*], *Mounir Jaidann* [b], *Louis-Simon Lussier* [b]

[a] *Department of Mechanical and Materials Engineering, University of Western Ontario, London, ON, Canada, N6A 5B9*
[b] *Defense Research and Development Canada – Valcartier, 2459 Boulevard PieXI Nord, Québec, QC, Canada G3J 1X5*

ARTICLE INFO

Article history:
Received 22 June 2009
Accepted 20 December 2009
Available online 28 December 2009

ABSTRACT

Nitrogen-doped carbon nanotubes (CN_x–NTs) were prepared using a floating catalyst chemical vapor deposition method. Melamine precursor was employed to effectively control nitrogen content within the CN_x–NTs and modulate their structure. X-ray photoelectron spectroscopy (XPS) analysis of the nitrogen bonding demonstrates the nitrogen-incorporation profile according to the precursor amount, which indicates the correlation between the nitrogen concentration and morphology of nanotubes. With the increase of melamine amount, the growth rate of nanotubes increases significantly, and the inner structure of CN_x–NTs displayed a regular morphology transition from straight and smooth walls (0 at.% nitrogen) to cone-stacked shapes or bamboo-like structure (1.5%), then to corrugated structures (3.1% and above). Both XPS and CHN group results indicate that the nitrogen concentration of CN_x–NTs remained almost constant even after exposing them to air for 5 months, revealing superior nitrogen stability in CNTs. Raman analysis shows that the intensity ratio of D to G bands (I_D/I_G) of nanotubes increases with the melamine amount and position of G-band undergoes a down-shift due to increasing nitrogen doping. The aligned CN_x–NTs with modulated morphology, controlled nitrogen concentration and superior stability may find potential applications in developing various nanodevices such as fuel cells and nanoenergetic functional components.

1. Introduction

Carbon nanotubes (CNTs) have been extensively studied in terms of both fundamental such as band structure and chirality [1], and practical applications such as electronics, optics, and energy conversion [2,3]. Due to the presence of additional lone pairs of electrons, nitrogen atoms can contribute additional electrons and provide electron carriers for the conduction band [4], which makes nitrogen-doped carbon nanotubes (CN_x–NTs) either metallic or narrow energy gap semiconductors [5]. Hence, nitrogen doping has been considered as a feasible strategy in a well-defined way for tuning physical and chemical properties of CNTs [6,7]. More recent study has indicated that CN_x–NTs with vertical alignment can effectively enhance the electrocatalytic activity of the nanotubes in terms of fuel cells applications [8]. On the other hand, first-principle simulations have shown that carbon nanotubes may be used to stabilize polymeric nitrogen or matrices for polynitrogen doping to form nanoscale energetic materials [9,10]. However, there exist some challenges during the synthesis of such nanoscale energetic materials because polynitrogen or polymeric nitrogen is not stable at ambient

* *Corresponding authors:* Fax: +1 519 661 3020, +1 418 844 4646.
E-mail addresses: xsun@eng.uwo.ca (X. Sun), hakima.abou-rachid@drdc-rddc.gc.ca (H. Abou-Rachid).
0008-6223/$ - see front matter
doi:10.1016/j.carbon.2009.12.045

condition. It is believed that the increasing nitrogen doping percent onto carbon nanotubes may have more opportunities to form polymeric nitrogen or polynitrogen in general [10].

Therefore, exploration of CN_x–NTs with tuning nitrogen concentration, modulated structure, and satisfying alignment would doubtlessly favor applications of the nanotubes in different fields such as fuel cells [11] and nanoenergetic materials [12].

Until now, many methods have been exploited to synthesize CN_x–NTs with controlled composition [13,14]. Recently, some interesting progresses have been made in controlling the morphology and structure of CN_x–NTs using different liquid nitrogen precursors by aerosol method [15–17]. And the relationship between the precursor amount and morphology of low nitrogen doped (0–2.2%) carbon nanotubes has been addressed. By using the mixture of benzylamine and toluene, Koós et al. [15] reported that the length and diameter of the nanotubes decrease with nitrogen concentration while bamboo shaped nanotubes increases. By using a mixture of ethanol/acetonitrile, Ayala et al. [16] found that single and multiwalled CN_x–NTs can be selectively grown by modulating the concentration of acetonitrile. Besides these techniques, the floating catalyst method has been regarded as a convenient way to ensure continuous growth of aligned CN_x–NTs with variable nitrogen concentration, which is crucial to modify the electrical and mechanical properties of the nanotubes [18–20].

Melamine ($C_3N_6H_6$) is a low-cost industrial material with a honey-comb atomic arrangement. Differing from the novel graphene with two-dimensional honey-comb structure [21], melamine possesses a three-dimensional monoclinic structure which is similar to C_3N_4 [22]. Due to its specific skeleton of CN heterocycles [23], catalytic decomposition of melamine can generate pre-existing C–N bonds, which favors the incorporation of nitrogen in CNTs [24]. Melamine has been employed as an effective precursor to prepared CN_x–NTs with high alignment [25]. However, influence of melamine on morphology, structure and nitrogen doping extent of CN_x–NTs has rarely been reported. In addition, melamine usually acts as the only carbon source during the growth of CN_x–NTs to maintain nitrogen content (generally <11%) within the CN_x–NTs due to the higher thermodynamic stability of carbon and separate nitrogen molecules at high temperature [26], which inevitably limits the scale-up growth of CN_x–NTs. On the other hand, CN_x–NTs with high nitrogen concentration generally display severe nitrogen loss after synthesis due to the weakly physisorbed N_2 molecules within the nanotubes [23].

In this work, bulk growth of multiwalled CN_x–NTs with good alignment, superior stability, modulated nitrogen concentration (0–8.4%) and resultant morphological changes (regular straight → cone stacked → corrugated tubular structure) have been obtained using a mixture of ethylene, melamine and ferrocene as the extra carbon source, nitrogen additive and catalyst precursor, respectively, in the floating catalyst chemical vapor deposition method. Through the analysis of the bonding environment of the nitrogen and the size dependence of the CN_x–NTs on the nitrogen, the issues related to nitrogen-incorporation profile according to the precursor amount and morphological control of CN_x–NTs is discussed.

2. Experimental

Before CN_x–NTs were grown on a silicon wafer substrate, the substrate was sputtered with a thin aluminum buffer layer (thickness 30 nm), which can arise a rough surface absorbing iron atoms into the traps of the alumina layer forming uniform and well-dispersed catalytic particles to obtain uniform and high density CN_x–NTs [27]. The sputtering was carried out under a pressure of 4.0 mTorr and at a power of 300 W.

The floating catalyst method was applied to synthesize CN_x–NTs based on a simple horizontal quartz tube furnace system. $Fe(C_5H_5)_2$ (100 mg, 98%, Aldrich) was placed at the entrance of the furnace in the quartz tube as the precursor to produce metallic iron particles as catalysts. Different amounts of melamine (99+%, Aldrich) were placed beneath the ferrocene as the nitrogen additive. A small piece of silicon wafer (1 cm × 3 cm) with 30 nm-thick aluminum buffer layer was located in the center of the oven.

Before the furnace was heated, Argon (99.999% in purity) was introduced into the heating system at a flow rate of 500 sccm for 30 min to displace the air in the tube. Then the system was heated to 850 °C at a rate of 60 °C/min. In this case, the temperature at the furnace entrance reached 200 °C, which is suitable for ferrocene evaporation. At the same time, ethylene gas was introduced into the system at a flow rate of 10 sccm. Thus the ferrocene vapor was carried by the gas flow into the high temperature region where the pyrolysis and synthesis occurred at 850 °C. The whole system was kept at the target temperature for 5 min. Then the furnace was heated to 950 °C. The temperature of the furnace entrance increased to 350 °C as the target temperature went higher. Melamine was evaporated at this temperature. The melamine vapor was brought into the reaction chamber by argon and it was pyrolyzed in the middle of the reaction chamber as the nitrogen additive. After 15 min, the ethylene gas was turned off and the system cooled down to room temperature in the flowing Ar gas.

The samples were characterized by various analysis techniques including Hitachi S-4500 field-emission scanning electron microscopy (SEM) operated at 5.0 kV, Philips CM10 transmission electron microscopy (TEM) operated at 80 kV, Kratos Axis Ultra Al(alpha) X-ray photoelectron spectroscopy (XPS) operated at 14 kV, a Horiba Jobin Yvon high resolution (HR800) confocal Raman spectrometer operated with an incident laser beam at 632.8 nm and a CHN elemental analyses were performed using a Perkin–Elmer PE244 analyser with oxygen for the combustion of the samples.

3. Results and discussion

3.1. *Morphological, nitrogen doping characterization and stability of the CN_x–NTs*

Fig. 1(a–f) shows typical SEM images of the CN_x–NTs obtained from 50 to 2000 mg melamine, respectively. It can be seen that the silicon wafer is totally covered by a film of aligned nanotubes with high density. With increasing melamine amount, the growth rate increases from 4 μm/min (50 and 200 mg melamine) to 5 μm/min (400 mg melamine), 7 μm/min (800 mg

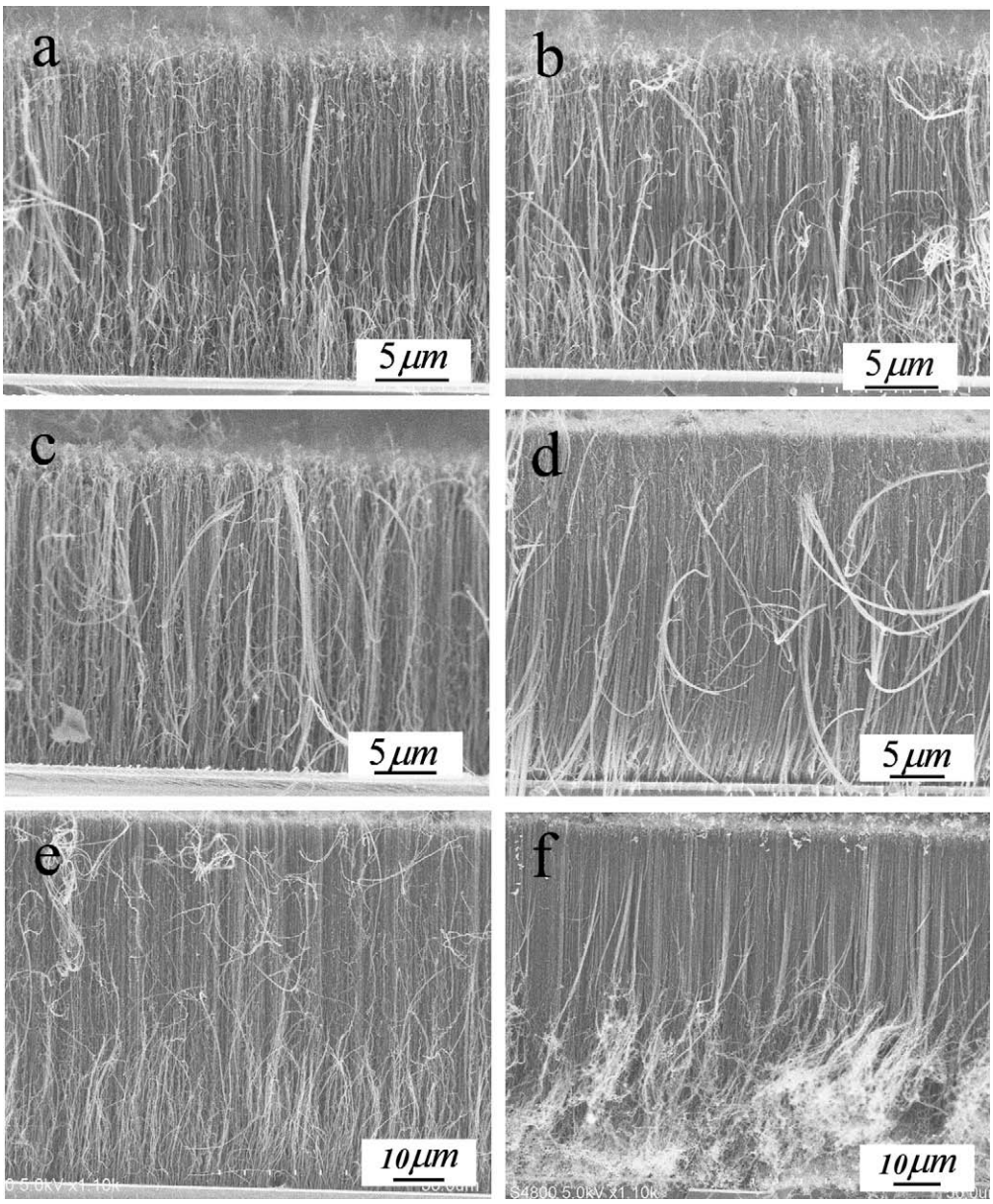

Fig. 1 – SEM images of N-CNTs synthesized with melamine amount of (a) 50 mg, (b) 200 mg, (c) 400 mg, (d) 800 mg, (e) 1500 mg and (f) 2000 mg.

melamine), and up to 14 μm/min (1500 and 2000 mg melamine). This is different from the growth using benzylamine as the nitrogen precursor [15], in which the growth rate of CN_x–NTs was slowed down with the precursor amount due to the nitrogen saturation at the growth end of the tube edge. In our growth process, decomposition of ethylene produces hydrogen, which could etch away carbon atoms on the catalyst. When nitrogen is involved by introducing melamine, the atomic nitrogen would abstract considerable amount of hydrogen atoms and retard the etching of carbon growth on the catalyst [28], thereby enhance the growth rate of the nanotubes.

In order to investigate the relation between morphology of the CN_x–NTs, incorporated nitrogen concentration and employed melamine amount, XPS and TEM characterizations were carried out. In XPS measurement, the N concentration present in the nanotubes, defined as atomic percent of nitrogen with respect to carbon, is estimated by the area ratio of the nitrogen and carbon peaks. XPS measurement indicated that CN_x–NTs with the atomic nitrogen concentration of 1.5%, 3.1%, 5.4%, 8% and 8.4% were obtained by using the melamine amount of 200, 400, 800, 1500 and 2000 mg. No nitrogen was detected from the nanotubes with the melamine amount of 50 mg. Fig. 2(a) shows C1s spectra of the nanotubes with different nitrogen concentration. The position of the main C1s line at 284.3–284.7 eV proves the graphite structure of the carbon [29]. The C1s peak at 284.3 eV corresponds to the energy of the sp^2 C–C bond in C1s spectrum of pyrolytic graphite [14]. With increasing melamine amount, the peak is shifted to higher binding energies of 284.6–284.7 eV, which is interpreted by disordering of the graphite-like structure after introduction of nitrogen [30].

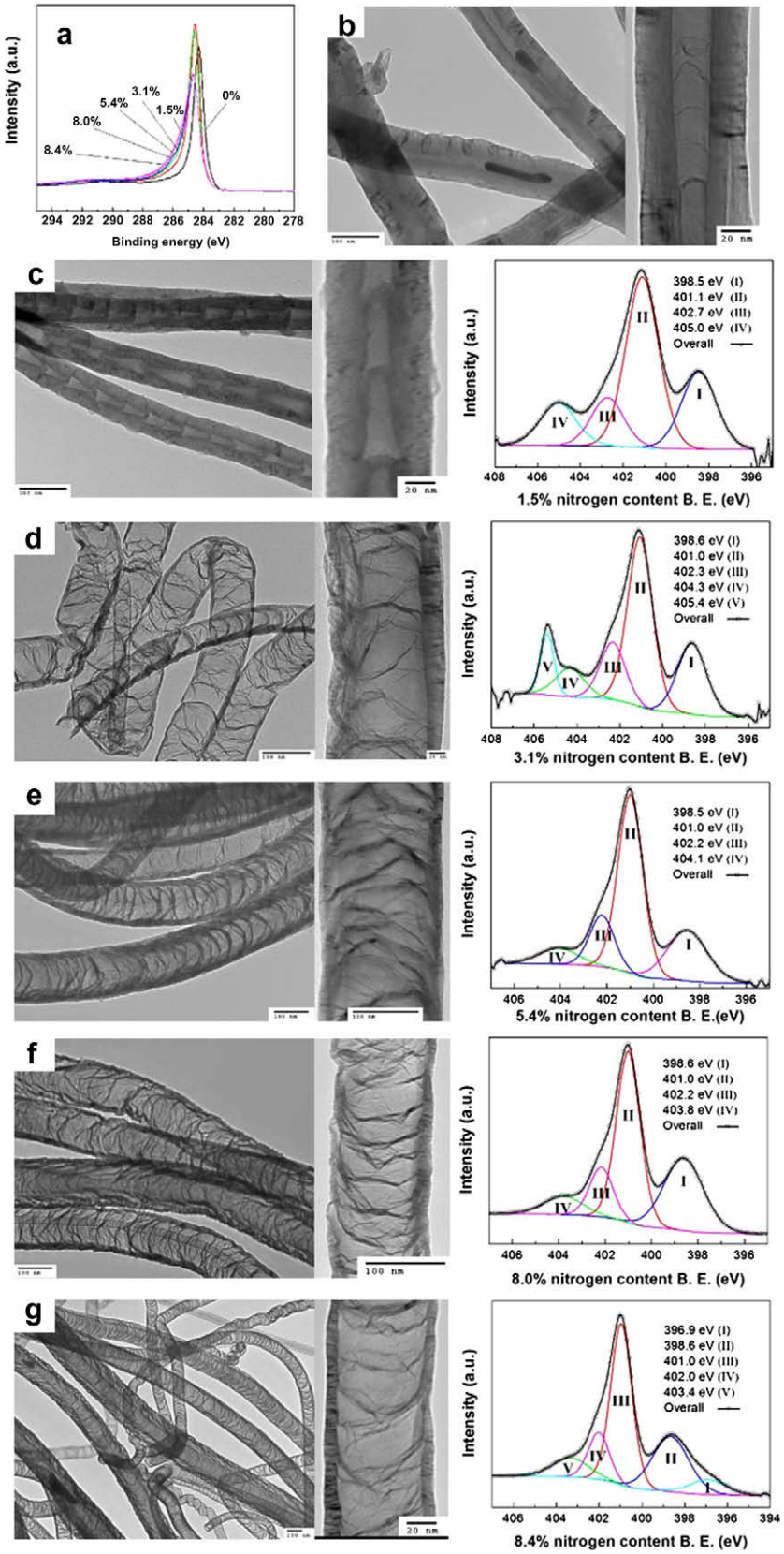

Fig. 2 – (a) XPS C1s spectra of CN_x–NTs with different nitrogen content, TEM images and related XPS N1s spectra (if applicable) of CN_x–NTs synthesized with nitrogen content of (b) 0%, (c) 1.5%, (d) 3.1%, (e) 5.4%, (f) 8.0% and (g) 8.4%. Inset: increased magnifications.

Fig. 2(b) shows typical TEM images of the carbon nanotubes using 50 mg melamine, no nitrogen can be detected from XPS. The morphology of CN_x–NTs remains almost unchanged compared to regular carbon nanotubes; only a few bamboo-like structures can be observed. Interlinks in the nanotubes are very thin and the outer diameter of the nanotubes is around 60–80 nm, while the wall thickness is around 20–30 nm.

With increasing melamine amount, CN_x–NTs with different nitrogen concentration were obtained. Left panel of Fig. 2(c)–(g) shows TEM observation of the CN_x–NTs with different melamine amount. TEM observations indicate that roughness and density of bamboo-like structure tend to increase with the melamine amount, which is similar to the previous report using benzylamine as the nitrogen precursor [15]. However, outer and inner diameter of the nanotubes increases with the melamine amount, differing from their case, in which outer diameter of the nanotube decreased while inner diameter increased with the benzylamine amount. Nevertheless, the wall thickness tends to decrease with increasing nitrogen precursor amount in both cases. When the melamine amount of 200 mg was used, as shown in Fig. 2(c), morphology of the nanotubes (nitrogen: 1.5%) becomes compartmentalized by lateral segmentations. It looks like many cones stacked together with the axes oriented in the same direction. The outer diameter of the nanotubes was still around 60–80 nm, not showing obvious size changes, and the wall thickness is still as thick as 20 nm. With increase of melamine to 400 mg (nitrogen: 3.1%), TEM image in the left panel of Fig. 2(d) shows that the nanotubes exhibit an irregular and inter-linked corrugated morphology. Comparing with the samples shown in Fig. 2(b) and (c), the diameter of these nanotubes tends to be much larger. The outer diameter reaches as large as 100–120 nm and the wall thickness decreases to 10–20 nm. With the increase of the melamine amount to 800 mg, 1500 mg, 2000 mg, CN_x–NTs with the nitrogen amount of 5.4%, 8% and 8.4% were obtained, respectively. As shown in the left panel of Fig. 2(e–g), compared to the nanotubes with 3.1%N, the outer diameter does not change much whereas the wall thickness decreases continuously down below 10 nm.

Plots in the right panel display high resolution N1s XPS spectra of the samples the same as those corresponding to the left panel, in which bonding environment and electronic structures of the nitrogen species were evaluated. The asymmetric N1s spectra indicate the existence of four or five components in each spectrum, which are fitted into peaks at 398.5–398.6 eV (N1), 401.0–401.1 eV (N2), 402.0–402.9 eV (N3), 396.9 eV (N4), 403.4–404.3 eV (N5), and 405.0–405.2 eV (N6), respectively. The peaks at 398.5–398.6 eV and 401.0–401.1 eV correspond to pyridine-like nitrogen and graphite-like nitrogen [13,31], respectively. The peak N3 is commonly attributed to oxidized nitrogen [32,33]. The three components appear in all N1s spectra of right panel with different nitrogen concentration. Based on the N1s spectra, detailed distribution of nitrogen composition has been summarized in Table1. Pyridine-like nitrogen atoms, contribute to the Π system with a pair of π electrons and only bonded to two C atoms (C–N=C), which has been proposed an essential component in generating bamboo-like structures [31]. It can be seen that the ratio of pyridine-like nitrogen tends to increase with increasing nitrogen concentration and reach its maximum in the nanotubes containing 8% nitrogen. This may interpret the increased corrugation density with the melamine amount. Further increasing the amount of melamine to 2000 mg does not result in more morphological changes, shown in Fig. 2(f). Similar to the reports previously [13,14], the morphology changes in the nanotubes can be attributed to the difference of nitrogen concentration within the nanotubes.

On the other hand, N4, N5 and N6 components are present or absent depending on the nitrogen concentration. For the CN_x–NTs with nitrogen concentration of 1.5%, as shown in the right panel of Fig. 2(c), the N1s spectrum can be fitted into four peaks at 398.5 eV, 401.1 eV, 402.7 eV, and 405 eV, in which we ascribe the peak at 405 eV to chemisorbed nitrogen oxide on the graphite layers [34]. In the case of the CN_x–NTs (3.1%N) with the melamine amount of 400 mg, as shown in the right panel of Fig. 2(d), position of four peaks at 398.6 eV, 401 eV, 402.3 eV, and 405.4 eV, is consistent with the case in the CN_x–NTs with 1.5%N; whereas one new peak at 404.3 eV appears. We attribute this peak to molecular nitrogen encapsulated or intercalated in the nanotubes. Previous reports have indicated that molecular nitrogen can be encapsulated inside the tubes [17,35] or exist as intercalated form between the graphite layers [19] during the growth of CN_x–NTs, and the intercalated molecular nitrogen distributes mainly at inner walls of the nanotubes, in which the N1s binding energy for free nitrogen gas is lowered due to extra atomic screening effect between N1s core hole and matrix [19]. With respect to the photon energy of 1486.6 eV used in our XPS measurement, the average probing depth should be below 10 nm. The wall thickness of CN_x–NTs (1.5%N) is over 20 nm, so the peak of molecular nitrogen is not detected. For the nanotubes with 3.1%N, wall thickness of the nanotubes decreases to 10–20 nm. It is possible to probe the electronic structure of nitro-

Table 1 – Detailed distribution of nitrogen composition.

Nitrogen concentration (at.%)	Area composition of different N structure (%) sorted by peak position (eV)					
	396.9	398.5–398.6	401–401.1	402–402.9	403.4–404.3	405–405.4
0	–	–	–	–	–	–
1.5	–	23.8	48.9	13.8	–	13.5
3.1	–	22	45.2	15.3	8.8	8.6
5.4	–	24.1	53.0	15.3	7.7	–
8.0	–	32.4	46.1	13.3	8.2	–
8.4	7.1	26.3	44.5	12.9	9.2	–

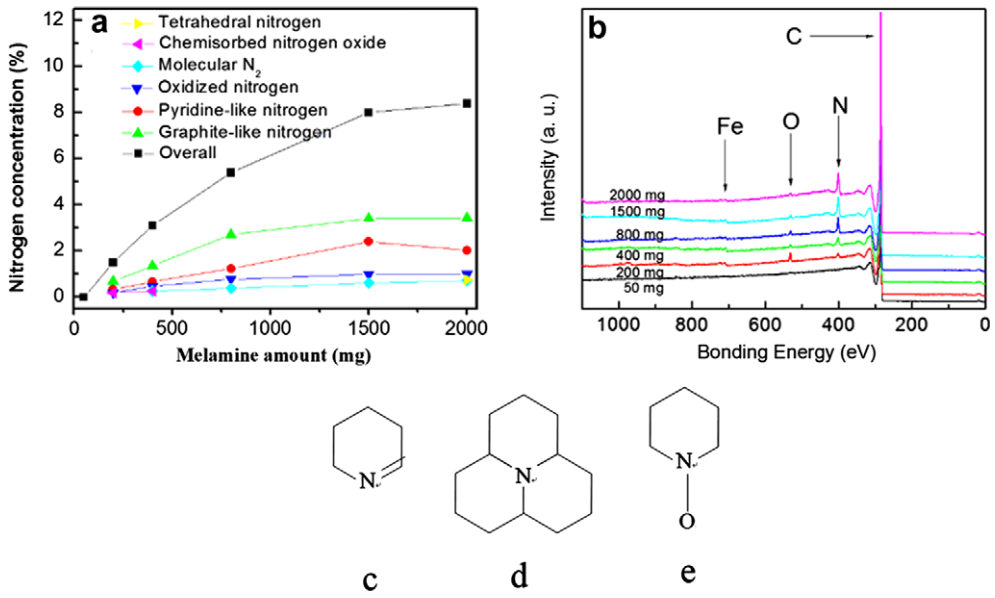

Fig. 3 – (a) Nitrogen content and composition of different nitrogen species in CN_x–NTs as a function of melamine amount, (b) XPS survey scan spectra of CN_x–NTs synthesized with different melamine, and nitrogen species found in nitrogen-doped carbon nanotubes: (c) pyridine-like nitrogen, (d) graphite-like nitrogen, and (e) oxidized nitrogen.

gen atoms at the inner walls which may contain encapsulated nitrogen or intercalated nitrogen, and the peak centered at 404.3 eV appears.

When the melamine amount was increased to 800, 1500 and 2000 mg, the deconvolution of the N1s spectra of the three cases gives rise to five nitrogen peaks, as shown in the right panel of Fig. 2(e–g), while the peak of molecular nitrogen centered at 403.4–404.1 eV appears in all the three spectra, the peak of chemisorbed nitrogen oxide is absent. In addition, a new peak at 396.9 eV is detected from the nanotubes with 8.4% nitrogen concentration. This peak can be assigned to the tetrahedral nitrogen bonded to sp^3-C probably due to un-decomposed N–H bond when excessive amount of melamine is used, which is similar to the case using octadecylamine as the precursor [36]. Based on the data in Table1, Fig. 3(a) demonstrates the nitrogen-incorporation profile according to the precursor amount. The ratio of graphite-like nitrogen reaches its maximum at the melamine amount of 800 mg (nitrogen: 5.4%) and decreases with further increasing melamine amount. The ratio of pyridine-like nitrogen keeps increasing until the melamine amount of 1500 mg (nitrogen: 8.0%). The ratio of nitrogen oxide and gaseous nitrogen is relatively low and stable, but the molecular nitrogen tends to increase slightly with the melamine amount. Graphite-like nitrogen atoms, shown in Fig. 3(d), substitute for carbon atoms in the hexagon graphene layers bonding to three carbon atoms. It is evident that the nitrogen atoms are incorporated into the carbon nanotubes mainly in pyridine-like and graphite-like ways in all cases. Due to higher stability of graphite-like nitrogen than that of pyridine-like nitrogen, while a small amount of melamine was introduced, the N atoms preferably take substitutional positions in the hexagon graphene and tend to be more graphite-like [37]. When more melamine is introduced into the reaction, the intensity ratio of *I*(pyridine-like nitrogen)/*I*(graphite-like nitrogen) increases. This suggests that more melamine can contribute more pyridine-like structure doping into the carbon nanotube lattice and increase the nitrogen concentration inside the nanotube, which may be associated with the pre-existing C–N bonds derived from the catalytic decomposition. It is believed that the nitrogen doping in the pyridine-like N sites is responsible for both the wall roughness and inter-linked morphologies, which is also in agreement with our TEM observation. In general, the nitrogen concentration increases intensively at the beginning. Depending on the precursor type, incorporation limit of nitrogen within carbon nanotubes has been previously investigated [16,30,38], it has been calculated that nitrogen doping of inner walls of the carbon nanotubes is more thermodynamically stable than the doping of out walls. In our case, a similar problem is encountered: the nitrogen concentration reaches its maximum as the melamine amount reaches 1500 mg, beyond which the nitrogen concentration increased much more slowly. Increasing melamine amount from 1500 mg to 2000 mg, it resulted only about 0.3% increase in nitrogen concentration. This indicates a challenge to achieve a significant further increase of the nitrogen doping using this method. It is possible that incomplete decomposition of excessive melamine is another reason.

A typical XPS survey scan of the CN_x–NTs using different amounts of melamine is shown in Fig. 3(b). The main peaks in these figures are distinguished as C1s, N1s, O1s and Fe2p signals, corresponding to main peaks centered at 285 eV, 401 eV, 531 eV and 708 eV, respectively. The strong C peak can be assigned to sp^2-hybridized carbon, which is the major component in CN_x–NTs. The N peak has been discussed above. The O peak occurs mainly due to the organic compounds containing C–O functionalities [39], the oxygen absorbed on the surface of the carbon nanotubes, and the substrate on which the nanotubes were grown [40]. The Fe peak arises from the catalyst, which is decomposed from ferrocene.

To further study the N/C nitrogen concentration and nitrogen stability in our CN_x–NTs, both as-synthesized samples and the samples exposed to air for 5 months were characterized by a CHN analyzer. Fig. 4(a) shows the nitrogen concentration dependence on the melamine amount in both as-synthesized and aged state. The measurement is carried out on whole samples. The nitrogen content are 1.3%, 3.2% and 4.5% separately for the as-synthesized samples using 200 mg, 800 mg and 2000 mg of melamine, which is lower than the N amount measured using XPS technique. However, the average nitrogen concentration reveals a similar trend of increase when compared with the trend observed from XPS spectra, further confirming an important role of the amount of nitrogen precursor in the reaction. The difference in measured nitrogen amount between the XPS analysis and CHN analysis is associated with feature of two techniques. XPS is a surface sensitive measurement technique while CHN detect all samples as a whole. In our experiment section, we mentioned that the nitrogen was introduced into the oven later than the catalyst precursors. Then, at the beginning of the experiment, non-doped CNTs were produced during the first several minutes of the experiment. Then the CN_x–NTs began to form when melamine was introduced. The experimental process results in non-uniform CN_x–NTs structures consisting of CN_x–NTs on the upper surface and general CNTs on below. As a surface method, XPS revealed extensive information from CN_x–NTs on the top, while CHN give us the information of the whole composite CN_x–NTs/CNTs film on substrate. Hence, it is reasonable to expect that the CHN would show a relatively lower nitrogen concentration than XPS.

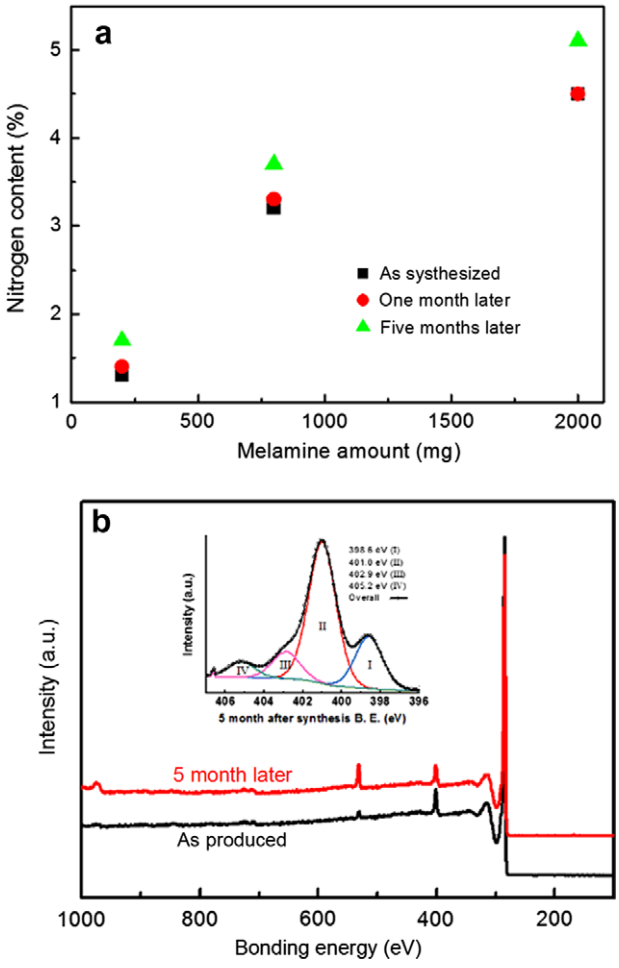

Fig. 4 – CHN spectra and XPS analysis of the samples at different time: (a) CHN analysis results of different sample at different times after synthesis (b) XPS spectra of the sample using 800 mg melamine taken soon after experiment and 5 months later, separately. Inset: XPS N1s spectrum of CN_x–NTs 5 months after synthesis.

It has been reported that nitrogen will release to some extent when CN_x–NTs are exposed to air [35]. In our case, as shown in Fig. 4(a), CHN results do not show evident change in nitrogen concentration with time at room temperature. The slight difference observed is due to the accuracy of the instrument. Fig. 4(b) shows the XPS survey spectra of the sample containing 5.4%N taken soon after the experiment and 5 months later. It indicates that total nitrogen concentration remains almost unchanged, which is consistent with the observation from CHN, however there is a great increase of oxygen. High resolution N1s spectra of the 5.4%N sample is shown in the inset image of Fig. 4(b). After exposing the sample to air for 5 months, there is almost no variation in the electronic structure of the pyridine-like and graphite-like nitrogen. The molecular peak at 404.1 eV disappears, implying the release of the N_2 from the graphite layers during the aging process, however, the peak at 405.2 eV appears, which has been ascribed to the peak of chemisorbed nitrogen oxide. This peak shift may due to the oxidation of the nitrogen species inside the graphite layers during the aging of the sample, which is consistent with the great increase of oxygen in the sample. Based on above analysis, total nitrogen concentration of the CN_x–NTs can be stably maintained though the bond of nitrogen species inside the CN_x–NTs may change during the aging process.

3.2. *Correlation between the nitrogen content and crystallinity of CN_x–NTs structures*

Fig. 5 shows typical HRTEM images of the CN_x–NTs with low and high nitrogen content of 1.5% and 8.4%, respectively. Generally, CN_x–NTs possess a rougher surface compared to non-doped CNTs. At lower nitrogen concentration of 1.5%, as shown in Fig. 5(a), the graphite cylinders still exhibit a relatively high degree of crystallinity in spite of the nanotube wall distortion resulting from the regular joint defects. Due to the decrease of the wall thickness from joint section to the base of the compartment, many open graphite edges are observed on the outer surface of nanotubes [41]. At high nitrogen concentration of 8.4% in Fig. 5(b), it can be seen that the crystallinity of the CN_x–NTs decreases significantly and the kinks inside the nanotube become random. The corrugated morphology and weak crystallinity of the CN_x–NTs imply a higher defect density with increasing nitrogen content, the origin of which may associated with the presence of pyridinic or other nitrogen [42], and is consistent with our XPS results.

To obtain information regarding the nitrogen doping and crystallinity of the entire CN_x–NTs, Raman spectra of the CN_x–NTs with three selected nitrogen contents (1.5%, 5.4% and 8.4%) are plotted. Two first-order Raman spectra of the

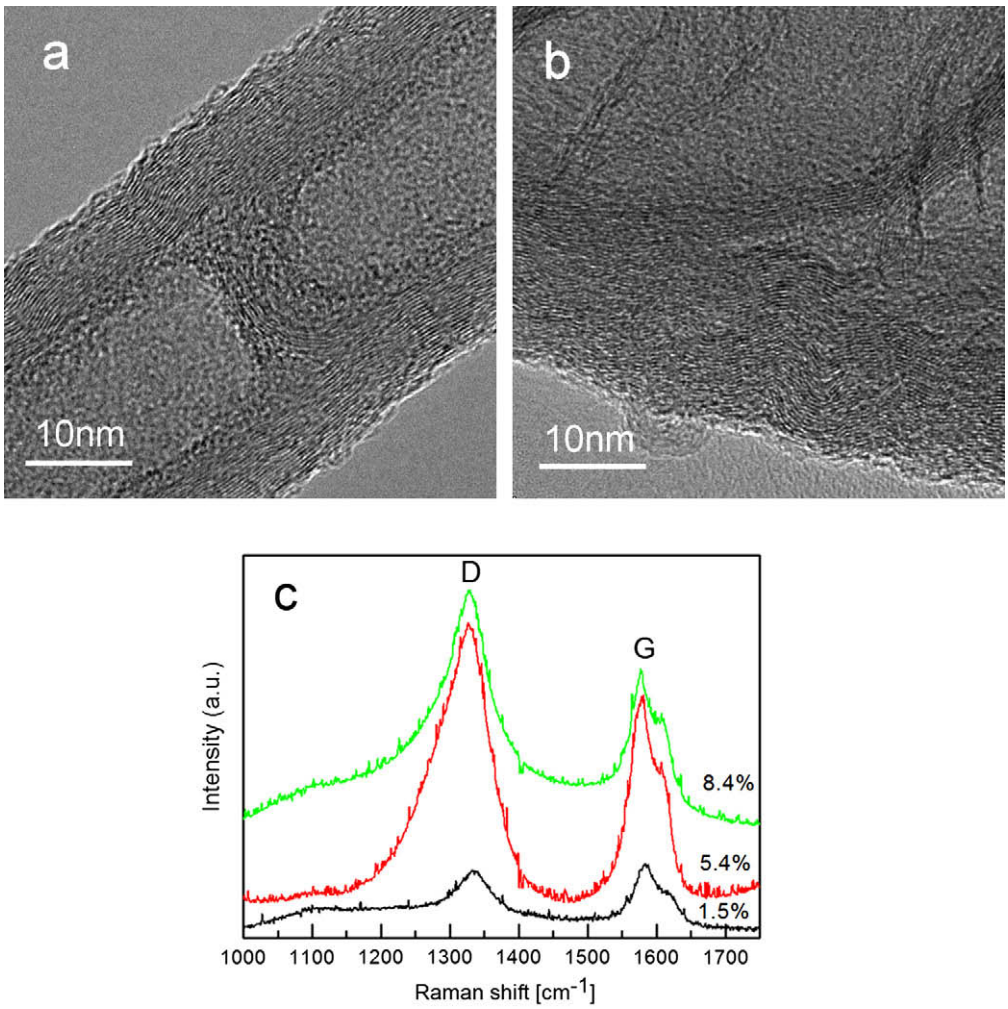

Fig. 5 – HRTEM images of the CN_x–NTs with the nitrogen content of (a) 1.5 at.% and (b) 8.4 at.% and (c) Raman spectra of CN_x–NTs with the nitrogen content of 1.5%, 5.4% and 8.4%.

samples are shown in Fig. 5(c). The bands at ~1315–1333 cm^{-1} (D-band) are originated from atomic displacement and disorder induced features caused by lattice defect, distortion or the finite particle size [43]. The band at ~1565–1582 cm^{-1} (G_1: 1582 cm^{-1}, G_2: 1575 cm^{-1}, G_3: 1565 cm^{-1}) indicates the formation of well-graphitized carbon nanotubes [44]. It is obvious that G-band of the CN_x–NTs undergoes a down-shift from 1582 to 1565 cm^{-1} with the melamine amount from 200 to 2000 mg. The G-band represents the tangential mode vibrations of carbon atoms in graphene sheets, and shifts of the G-band have been ascribed to C–C expansion (or contraction) and the changes of electronic structure [45]. The nitrogen atoms can act as electron donors when CNTs are doped with nitrogen. In our case, the down-shift of the G-band with increasing nitrogen doping concentration (1.5–8.4%) may imply an enhanced electron transfer between valance and conduction bands, which is in accordance with the reported results [46]. On the other hand, the intensity ratio of D-band to G-band (I_D/I_G) is measured to be 0.897, 1.333 and 1.553 at the melamine amounts of 200, 800 and 2000 mg, respectively, revealing an increased intensity ratio with the melamine amount. This indicates that the degree of long-range ordered crystalline perfection of the CN_x–NTs decreases and more defects and disorders are introduced with more nitrogen doping amount, which coincides with the TEM observations of the structure transition from the bamboo structure with lower structure defect and distortion to the corrugated structure with greatly increased defects. This result also confirms our conclusion that the defects and disorders are related to the presence of nitrogen in the CNTs [13,14].

4. Conclusion

Aligned nitrogen-doped carbon nanotubes with tuned morphology and controlled nitrogen concentration (up to 8.4%) have been successfully synthesized on the silicon wafer via a simple floating catalyst CVD method. TEM observations indicated that the structure of the nanotubes changed from straight nanotubes (0%) to cone stacked structures as the nitrogen concentration was increased to 1.5%. Then the structure changed to inter-linked corrugated morphology when nitrogen concentration went still higher (3.1–8.4%). It is conceivable that the incorporated nitrogen significantly influences the structure of CN_x–NTs. XPS investigation reveals

that nitrogen content within the nanotubes increases almost linearly with melamine amount until 8.4% nitrogen content was achieved. The nitrogen-incorporation profile according to the precursor amount indicates that while the content of graphite- and pyridine-like nitrogen experiences a maximum value with increasing nitrogen doping, the molecular nitrogen tends to increase slowly, which provides interesting information to interpret the upper limit of the nitrogen doping during the CN_x–NTs growth in our case. Both XPS and CHN results indicate that the nitrogen in carbon nanotubes is highly stable even after exposing the sample in air for 5 months. Raman scattering spectra suggest that the increase of nitrogen doping would result in more defects within the CN_x–NTs and implies an enhanced electron transfer between valance and conduction bands. The aligned CN_x–NTs with modulated morphology, controlled nitrogen concentration and superior stability may find potential applications in developing various nanodevices such as fuel cells and nanoenergetic functional components.

Acknowledgements

This research was supported by Department of National Defense (DND), Natural Sciences and Engineering Research Council of Canada (NSERC), Canada Research Chair (CRC) Program, Canada Foundation for Innovation (CFI), Ontario Research Fund (ORF), Ontario Early Researcher Award (ERA) and the University of Western Ontario. We are in debt to David Tweddell, Fred Pearson, Ronald Smith, Mark Biesinger, Ross Davidson and Todd Simpson for their kind help and fruitful discussions.

REFERENCES

[1] Anantram MP, Léonard F. Physics of carbon nanotube electronic devices. Rep Prog Phys 2006;69:507–61.
[2] Baughman RH, Zakhidov AA, De Heer WA. The route toward applications science. Carbon Nanotubes 2002;297(2):787–92.
[3] Villers D, Sun SH, Serventi AM, Dodelet JP, Desilets S. Characterization of Pt nanoparticles deposited onto carbon nanotubes grown on carbon paper and evaluation of this electrode for the reduction of oxygen. J Phys Chem B 2006;110(51):25916–25.
[4] Terrones M, Ajayan PM, Banhart F, Blasé X, Carrol DL, Charlier JC, et al. N-doped and coalescence of carbon nanotubes: synthesis and electronic properties. Appl Phys A 2002;74:355–61.
[5] Miyamoto Y, Cohen ML, Louie SG. Theoretical investigation of graphitic carbon nitride and possible tubule forms. Solid State Commun 1997;102(8):605–8.
[6] Chun KY, Lee HS, Lee CJ. Nitrogen doping effects on the structure behavior and the field emission performance of double-walled carbon nanotubes. Carbon 2009;47:169–77.
[7] Bian SW, Ma Z, Song W G. Preparation and characterization of carbon nitride nanotubes and their applications as catalyst supporter. J Phys Chem C 2009;113:8668–72.
[8] Gong KP, Du F, Xia Z, Durstock M, Dai L. Nitrogen-doped carbon nanotube arrays with high electrocatalytic activity for oxygen reduction. Science 2009;323:760–4.
[9] Abou-Rachid H, Hu A, Arato D, Sun X, Desilets S. Novel nanoscale high energetic materials: nanostructured polymeric nitrogen and polynitrogen. In: Kuo KK, Hori K, editors. Advancements in energetic materials and chemical propulsion. New York: Begell House, Inc.; 2008. p. 364–76.
[10] Abou-Rachid H, Hu A, Timoshevskii V, Yanfeng S, Lussier L-S. Nanoscale high energetic materials: a polymeric nitrogen chain N8 confined inside a carbon nanotube. Phys Rev Lett 2008;100:196401.
[11] Saha MS, Chen Y, Li R, Sun X. Enhancement of PEMFC performance by using carbon nanotubes supported Pt–Co alloy catalysts. Asia-Pac. J Chem Eng 2008;4(1):12–6.
[12] Rossi C, Zhang K, Esteve D, Alphose P, Tailhades P, Vahlas C. Nanoenergetic materials for MEMS: a review. J Micro Syst 2007;16(4):919–31.
[13] Tao XY, Zhang XB, Sun FY, Cheng JP, Liu F, Luo ZQ. Large-scale CVD synthesis of nitrogen-doped multi-walled carbon nanotubes with controllable nitrogen content on a $Co_xMg_{1-x}MoO_4$ catalyst. Diamond Relat Mater 2007;16(3):425–30.
[14] Maldonado S, Morin S, Stevenson KJ. Structure, composition, and chemical reactivity of carbon nanotubes by selective nitrogen doping. Carbon 2006;44(8):1429–37.
[15] Kóos AA, Dowling M, Jurkschat K, Crossley A, Grobert N. Effect of the experimental parameters on the structure of nitrogen-doped carbon nanotubes produced by aerosol chemical vapour depositions. Carbon 2009;47:30–7.
[16] Ayala P, Grüneis A, Kramberger C, Rümmeli M H, Solózano I G, Freire Jr F L, et al. Effect of the reaction atmosphere composition on the synthesis of single and multiwalled nitrogen-doped nanotubes. J Chem Phys 2007;127:1847091–6.
[17] Reyes-Reyes M, Grobert N, Kamalakaran R, Seeger T, Golberg D, Rühle M, et al. Efficient encapsulation of gaseous nitrogen inside carbon nanotubes with bamboo-like structure using aerosol thermolysis. Chem Phys Lett 2004;396:167–73.
[18] Nevidomskyy AH, Csanyi G, Payne MC. Chemically active substitutional nitrogen impurity in carbon nanotubes. Phys Rev Lett 2003;91(10):1055021–4.
[19] Choi HC, Bae SY, Park J, Seo K, Kim C, Kim B, et al. Experimental and theoretical studies on the structure of N-doped carbon nanotubes: possibility of intercalated molecular N_2. Appl Phys Lett 2004;85(23):5742–4.
[20] Costa PMFJ, Golberg D, Mitome M, Bando Y. Electrical properties of CN_x nanotubes probed in a transmission electron microscope. Appl Phys A 2008;90(2):225–9.
[21] Alwarappan S, Erdem A, Liu C, Li CZ. Probing the electrochemical properties of grapheme nanosheets for biosensing applications. J Phys Chem C 2009;113:8853–7.
[22] Alves I, Demazeau G, Tanguy B, Weill F. On a new model of the graphitic form of C_3N_4. Solid State Commun 1999;109(11):697–701.
[23] Li J, Cao C, Zhu H. Synthesis and characterization of graphite-like carbon nitride nanobelts and nanotubes. Nanotechnology 2007;18:1156051–6.
[24] Tang C, Bando Y, Golberg D, Xu F. Structure and nitrogen incorporation of carbon nanotubes synthesized by catalytic pyrolysis of dimethylformamide. Carbon 2004;42(12–13):2625–33.
[25] Terrones M, Terrones H, Grobert N, Hsu WK, Zhu YQ, Hare JP, et al. Efficient route to large arrays of CN_x nanofibers by pyrolysis of ferrocene/melamine mixtures. Appl Phys Lett 1999;75:3932–4.
[26] Badding JV, Nesting DC. Thermodynamic analysis of the formation of carbon nitrides under pressure. Chem Mater 1996;8(2):535–40.
[27] Liu H, Arato D, Li R, Zhang Y, Merel P, Sun X. Aligned multi-walled carbon nanotubes synthesized by floating catalyst CVD: effects of buffer layer and substrates. Surf Coating Tech 2008;202(17):4114–20.
[28] Lee JY, Lee BS. Nitrogen induced structure control of vertically aligned carbon nanotubes synthesized by microwave plasma

enhanced chemical vapor deposition. Thin Solid Films 2002;418:85–8.
[29] Pels JR, Kapteijn F, Moulijn JA, Zhu Q, Thomas KM. Evolution of nitrogen functionalities in carbonaceous materials during pyrolysis. Carbon 1995;33:1641–53.
[30] Ayala P, Grüneis A, Gemming T, Büchner B, Rümmeli MH, Grimm D, et al. Influence of the catalyst hydrogen pretreatment on the growth of vertically aligned nitrogen-doped carbon nanotubes. Chem Mater 2007;19:6131–7.
[31] Ayala P, Grüneis A, Gemming T, Grimm D, Kramberger C, Rümmeli MH, et al. Tailoring N-doped single and double wall carbon nanotubes from a nondiluted carbon/nitrogen feedstock. J Phys Chem C 2007;111:2879–84.
[32] Morant C, Anrey J, Prieto P, Mendiola D, Sanz JM, Elizalde E. XPS characterization of nitrogen-doped carbon nanotubes. Phys. Stat. Sol. (a) – Appl Mater Sci 2006;203(6):1069–75.
[33] Xu F, Minniti M, Barone P, Sindona A, Bonanno A, Oliva A. Nitrogen doping of single walled carbon nanotubes by low energy N_2^+ ion implantation. Carbon 2008;46:1489–96.
[34] Biniak S, Szymanski G, Siedlewski J, Swiatkowski A. Carbon 1997;35:1799–810.
[35] Choi HC, Bae SY, Jang WS, Park J, Song HJ, Shin HJ, et al. Release of N_2 from the carbon nanotubes via high-temperature annealing. J Phys Chem B 2005;109:1683–8.
[36] Ghosh K, Kumar M, Maruyama T, Ando Y. Micro-structural, electron-spectroscopic and field-emission studies of carbon nitride nanotubes grown from cage-like and linear carbon sources. Carbon 2009;47:1565–75.
[37] Hellgren N, Johansson MP, Broitman E, Hultman L, Sundgren JE. Role of nitrogen in the formation of hard and elastic CN_x thin films by reactive magnetron sputtering. Phys Rev B 1999;59(7):5162–9.
[38] Kim SY, Lee J, Na CW, Park J, Seo K, Kim B. N-doped double-walled carbon nanotubes synthesized by chemical vapor deposition. Chem Phys Lett 2005;413:300–5.
[39] Shalagina AE, Ismagilov ZR, Podyacheva OY, Kvon RI, Ushakov VA. Synthesis of nitrogen-containing carbon nanofibers by catalytic decomposition of ethylene/ammonia mixture. Carbon 2007;45(9):1808–20.
[40] He M, Zhou S, Zhang J, Liu Z, Robinson C. CVD growth of N-doped carbon nanotubes on silicon substrates and its mechanism. J Phys Chem B 2005;109(19):9275–9.
[41] Srivastava SK, Vankar VD, Sridhar Rao DV, Kumar V. Enhanced field emission characteristics of nitrogen-doped carbon nanotube films grown by microwave plasma enhanced chemical vapor deposition process. Thin Solid Film 2006;515(4–5):1851–6.
[42] Liu J, Webster S, Carroll DL. Temperature and flow rate of NH_3 effects on nitrogen content and doping environments of carbon nanotubes frown by injection CVD method. J Phys Chem B 2005;109(33):15769–74.
[43] Choi H, Park J, Kim B. Distribution and structure of N atoms in multiwalled carbon nanotubes using variable-energy X-ray photoelectron spectroscopy. J Phys Chem B 2005;109:4333–40.
[44] Dresselhaus MS, Dresselhaus G, Saito R, Jorio A. Raman spectroscopy of carbon nanotubes. Phys Rep 2005;409(2):47–99.
[45] Dresselhaus MS, Eklund PC. Phonons in carbon nanotubes. Adv Phys 2000;49:705–814.
[46] Yang QH, Hou PX, Unno M, Yamauchi S, Saito R, Kyotani T. Dual Raman features of double coaxial carbon nanotubes with N-doped and B-doped multiwalls. Nano Lett 2005;5(12):2465–9.